Cortico-cortical projections in mouse visual cortex are functionally target specific

Lindsey L Glickfeld[1], **Mark L Andermann**[1,2], **Vincent Bonin**[1,2], and **R Clay Reid**[1,2]
[1]Department of Neurobiology, Harvard Medical School, Boston, Massachusetts, USA

Abstract

Neurons in primary sensory cortex have diverse response properties, whereas higher cortical areas are specialized. Specific connectivity may be important for areal specialization, particularly in the mouse, where neighboring neurons are functionally diverse. To examine whether higher visual areas receive functionally specific input from primary visual cortex (V1), we used two-photon calcium imaging to measure responses of axons from V1 arborizing in three areas with distinct spatial and temporal frequency preferences. We found that visual preferences of presynaptic boutons in each area were distinct and matched the average preferences of recipient neurons. This specificity could not be explained by organization within V1 and instead was due to both a greater density and greater response amplitude of functionally matched boutons. Projections from a single layer (layer 5) and from secondary visual cortex were also matched to their target areas. Thus, transmission of specific information to downstream targets may be a general feature of cortico-cortical communication.

Individual neurons in mouse V1, like those of primates and carnivores, respond selectively to distinct features in visual scenes[1–6]. Unlike primate and carnivore visual cortex, rodent visual cortex lacks obvious functional architecture for features such as orientation and spatial frequency, so that neighboring neurons have distinct response properties[7,8]. This local heterogeneity suggests that precise synaptic connectivity might be required for the processing of sensory signals both within and between cortical areas[9,10].

Anatomical studies in primates have found that projections to different higher visual areas originate from different functional compartments, defined by cytochrome oxidase staining[11,12], cortical laminae[13,14] or cell types[15,16]. These anatomical distinctions between classes of projection neurons provide evidence for parallel information streams[17]. In the mouse, tracer studies suggest that disjoint (but spatially intermingled) populations of neurons in V1 project to different higher visual areas (ref. 18 and Q. Wang & A. Burkhalter, *Soc. Neurosci. Abstr.* 854.1, 2005). However, few studies in any species have found

evidence that neurons in close proximity make functionally specific interareal projections[19–22].

In the mouse, the densest cortico-cortical projections from V1 terminate in visual cortical areas LM (lateromedial), AL (anterolateral) and PM (posteromedial)[23]. Area LM is anatomically homologous to secondary visual cortex in primates[24], and neurons in this area, like those in V1, have a broad range of preferences for spatial and temporal frequency[4,5,25]. In contrast, neurons in areas AL and PM prefer distinct subsets of the range of spatial and temporal frequency preferences spanned by neurons in V1 (refs. 4–6). Neurons in AL respond best to stimuli with high temporal and low spatial frequencies (that is, quickly moving, coarse stimuli), whereas those in PM respond best to stimuli with low temporal and high spatial frequencies (that is, slowly moving, fine stimuli).

How these signals are transmitted from V1 to the higher visual areas is not known. One possibility is that the net input from V1 to each target area reflects the diverse visual response tuning of all V1 neurons (Fig. 1a, top). In this model each higher visual area receives the same input, and its functional properties may be determined through local computations. Alternatively, V1 may provide functionally distinct input to each downstream area (Fig. 1a, bottom). In this model, these target-specific projections could account for the specialization found in the higher visual areas.

To determine whether neurons in V1 make functionally target-specific synaptic inputs, we imaged visually evoked calcium signals in the axons of projection neurons. We found a marked target specificity of these projections, whereby each higher visual area receives functionally distinct sensory input from layers 2/3 and 5 of V1. Projections solely from layer 5 and secondary visual area LM were also functionally target specific, suggesting that the transmission of distinct sensory information to different cortical targets may be a general principle of cortical processing.

RESULTS

To determine the functional specificity of axonal projections from V1 to higher visual areas, we made targeted injections of a viral vector carrying the genetically encoded calcium indicator GCaMP3.3 (GCaMP3; see Online Methods) to posteromedial V1, which corresponds to the monocular region of the upper visual field[23]. Somatic GCaMP3 expression remained confined to V1, with most of the infected neurons less than 1 mm from the injection site (Fig. 1b,c and Supplementary Fig. 1a–c). Although expression in V1 spanned all lamina, the densest expression labeled neurons in layers 2/3 and 5 (Supplementary Fig. 1d, and see below). In fixed sections, labeled axonal projections were visible in the target areas surrounding V1 (Fig. 1b) and were densest in areas LM, AL and PM[23,26]. These arborizations likely arose from neurons in layers 2/3 and 5 of V1 and spanned all laminae in the higher visual areas[26] (Supplementary Fig. 1d). We rarely observed labeling of cell bodies in the higher visual areas, suggesting that there was little or no contamination by retrograde infection. We focused on areas LM, AL and PM because they receive the densest projections and because neurons in each of these areas have distinct receptive field properties[4].

Functional imaging of boutons in higher visual areas

We surgically implanted a chronic cranial window that provided optical access to V1 and the surrounding higher visual areas[4] so we could image the activity of labeled V1 axons in awake mice (Fig. 1c). During the experiments, mice were head-fixed and placed on a single-axis rotating ball on which they could run freely. Wide-field epifluorescence microscopy revealed bright islands of labeled axons in the higher visual areas. Registration to retinotopic

maps measured using intrinsic autofluorescence imaging confirmed the area identification for each mouse (Supplementary Fig. 1 and Online Methods). Using a high-speed two-photon microscope[8], we were able to measure visually evoked calcium transients from axonal arborizations in layers 1 and 2/3 (Fig. 1c,d and Supplementary Movie 1; average depth of imaging, 84.5 μm below the pia; range, 50–150 μm; 40 fields of view 200–300 μm on a side; 14 mice).

We studied the visual response properties of the axonal arborizations by presenting sinusoidal drifting gratings of different spatial and temporal frequencies (0.02 to 0.32 cycles per degree (c.p.d.); 1 to 15 Hz; 1-octave steps; 5 s off, 5 s on; see Supplementary Fig. 1f and Online Methods). Visual stimulation evoked calcium transients in axons coursing within the imaged plane (Fig. 1c–e and Supplementary Movie 1). Along these axonal processes were micrometer-sized hotspots that underwent local, visually evoked increases in fluorescence and likely corresponded to presynaptic boutons[27–29] (Fig. 1d; see Online Methods).

To quantify the selectivity of axonal responses in each area, we identified all visually responsive boutons in each field of view and determined their response profiles to all of the stimuli (Fig. 1e; see Online Methods). To visualize these two-dimensional tuning curves, we plotted a circle for each spatial and temporal frequency presented whose area was proportional to the amplitude of the response (dF/F). We then fit the profiles with a two-dimensional Gaussian function and considered only those boutons whose responses were well fit. These fits were used to estimate the preferred spatial and temporal frequencies for each bouton and to calculate the peak speed (the ratio of preferred temporal frequency to preferred spatial frequency), as this was the dimension that best segregated cell bodies in AL from those in PM[4].

The fluorescence images had high signal-to-noise ratios that enabled the resolution of responses in individual trials and repeatable measurements of the tuning of individual boutons (see Supplementary Movie 1, Supplementary Fig. 2e and Online Methods). Presentation of different visual stimuli evoked responses in distinct processes (Fig. 1c,d, Supplementary Fig. 2a and Supplementary Movie 2). This suggested that we were imaging axonal arborizations from multiple neurons in each field of view. To obtain a rough estimate the number of distinct processes, we measured the trial-by-trial correlations for all pairs of boutons in the field of view. We then used an unsupervised clustering algorithm to group correlated boutons that likely belonged to the same axonal process (Supplementary Fig. 2b,c). Pairs of boutons showing locally maximal correlations had nearly identical tuning and time courses, whereas those from different clusters often had different tuning and time courses (Supplementary Fig. 2d,e). From this analysis, we estimated that the 382 boutons in the experiment in Figure 1 arose from at least 15–20 functionally distinct axons.

Functional specificity of boutons in higher visual areas

We measured the spatial and temporal frequency tuning from 8,085 axonal boutons in the three higher visual areas (LM: 2,252 boutons, 9 mice, 11 fields of view; PM: 3,931 boutons, 12 mice, 15 fields of view; AL: 1,902 boutons, 12 mice, 14 fields of view). Although the stimulus preferences of V1 axons in each field of view were diverse (Fig. 2a), each of the three areas showed, on average, distinct preferences for spatial and temporal frequency (Fig. 2b,c). V1 axonal boutons in AL responded more strongly to higher temporal frequencies and lower spatial frequencies, generating threefold larger responses at higher speeds (Fig. 2c,d; paired, two-tailed Student's t-test, comparison of dF/F of boutons in AL for the two lowest versus two highest frequencies and the three lowest versus three highest speeds: all P-values $< 10^{-50}$). In contrast, V1 axonal boutons in PM showed opposite biases, responding more strongly on average to lower temporal frequencies and to higher spatial frequencies, generating threefold larger responses at slower speeds (all P-values $< 10^{-50}$). In comparison,

the average input to LM was broadly tuned and did not respond selectively to either high or low spatial frequencies, and had only modestly stronger responses to lower temporal frequencies (spatial frequency, $P > 0.09$; temporal frequency, $P < 10^{-8}$; speed, $P < 10^{-4}$).

These differences in tuning were robust: the average tuning was more correlated across experiments within an area than between areas (correlation coefficient within an area, 0.45 ± 0.02, $n = 14$ mice, 169 pairs; between areas, 0.02 ± 0.04, $n = 14$ mice, 149 pairs; unpaired, two-tailed Student's t-test: $P < 10^{-13}$). Nor were these differences dependent on bouton selection, as they were present when considering all pixels in the field of view (Supplementary Fig. 3). These results suggest that the three major cortical targets of V1 receive distinct visual information. Specifically, we found that projections from V1 to AL and PM responded preferentially to fast and slow moving stimuli, respectively. On average, these preferences matched the functional properties of the neurons in these areas[4], suggesting that neurons in V1 make functionally target-specific projections.

Lack of functional organization for frequency preference

Functional target specificity has been observed in carnivores and primates; however, much of this specificity can be explained by local functional architecture, such as the specific targeting of higher visual areas by distinct layers[11–13]. To determine whether there is any local organization of frequency preference in mouse V1 that could explain the specificity we found, we measured the spatial and temporal frequency tuning of somata across layers 2/3 to 5 (Fig. 3). We collected tuning responses from 542 neurons in layer 2/3 ($n = 166$, four mice), layer 4 ($n = 64$, two mice) and layer 5 ($n = 312$, two mice) that were well fit by our model (Fig. 3a,b; see Online Methods). Consistent with previous electrophysiological studies[2], we found no difference in peak speed across these layers and no evidence for clustering either across depth or in the tangential plane (Fig. 3c–e; tuning distance (the difference in peak speed for a pair of neurons normalized by the range of speeds presented; see Online Methods) across z and x-y distance, $n = 56,931$ pairs, two mice, Wilcoxon rank-sum test corrected for multiple comparisons: all P-values > 0.05). Moreover, the population of neurons in layers 2/3 and 5, the main sources of the cortico-cortical projection[26], was broadly tuned (Fig. 3f) and showed no difference in the distribution of peak speeds (Fig. 3g; Kolmolgorov-Smirnov (K–S) test: $P > 0.3$). Thus, we found no evidence for local organization in V1 that could account for the functional differences in the projections to the higher visual areas.

Although the tuning properties of neurons in layers 2/3 and 5 are not functionally organized, the projections from each layer could be functionally distinct. To investigate the functional target specificity of projections originating from a single cortical layer, we took advantage of a Cre-recombinase bacterial artificial chromosome (BAC) transgenic mouse line (Rbp4-Cre) that selectively labels a subpopulation of neurons in layer 5. Cre-dependent reporter expression in V1 was restricted to a dense population in layer 5 and a much sparser subset of layer 6 (Fig. 4a). We then made injections of Cre-dependent GCaMP3.3 virus (see Online Methods) to functionally characterize this population of layer 5 neurons and their axonal projections (Fig. 4b).

Rbp4-Cre–expressing neurons showed a similar diversity of tuning and peak speeds to that seen in neurons of wild-type (WT) mice (Fig. 4b–d; WT: $n = 312$ neurons, two mice; Rbp4-cre: $n = 159$ neurons, two mice; K–S test: $P > 0.05$). Although the Rbp4-cre population made projections to all of the higher visual areas, the projections to LM and PM were notably denser than those to AL (Fig. 4e). Nonetheless, the functional target specificity of axonal projections still held in this subpopulation of layer 5 neurons (Fig. 4f,g; LM: 559 boutons, two mice, four fields of view; PM: 618 boutons, two mice; seven fields of view; AL: 28 boutons, one mouse, four fields of view). On average, the population of boutons in

PM preferred slower speeds (paired, two-tailed Student's *t*-test, comparison of d*F*/*F* of boutons in PM to the three lowest versus three highest speeds: $P < 10^{-50}$), whereas boutons in AL preferred faster speeds ($P < 10^{-8}$). In comparison, the populations of boutons in LM were broadly tuned ($P > 0.1$). Together, these data suggest that the projection of neurons to the higher visual areas reflects their function and not simply their anatomical location in V1.

Target specificity of projections to higher visual areas

Two factors might explain the distinct tuning properties of V1 projections to the higher visual areas. First, the boutons of V1 neurons functionally matched to the target area might outnumber those that are not matched (Fig. 5a, left). Second, functionally matched boutons could exhibit larger calcium responses, thereby making larger contributions to the average response (Fig. 5a, right).

Consistent with the first possibility, the distribution of boutons' preferred spatial and temporal frequencies differed substantially between target areas (Fig. 5b; K–S tests, AL versus PM, AL versus LM, and PM versus LM: all *P*-values $< 10^{-16}$ for spatial and temporal frequencies and speed). These differences in distribution were also present among the population of boutons arising selectively from layer 5 (Fig. 5c; K–S tests: all *P*-values $< 10^{-11}$). In both data sets, the median speed of boutons in PM was lower than the median speed in either LM or AL (Fig. 5d; paired, one-tailed Student's *t*-tests of median bouton speed between areas within mice: PM versus AL, *n* = 8, *P* < 0.01; PM versus LM, *n* = 9, *P* < 0.05; AL versus LM, *n* = 6, *P* > 0.05). Notably, we found a strong correspondence between the properties of the axons from V1 and the properties of cell bodies in the targeted areas[4]. The median speeds for axons and cell bodies were similar in both AL (73 versus 71 deg s^{-1}) and PM (20 versus 17 deg s^{-1}; Fig. 5d). These data support the hypothesis that V1 neurons with preferences matched to their target area are more likely to project to, or have larger arborizations in, that area.

However, the distribution of peak speeds for axonal boutons was more diverse than for cell bodies in AL and PM (Fig. 5d). This suggests that, in addition to the bias in fraction of boutons (Fig. 6a,b), there may be other factors underlying the observed target specificity. Indeed, consistent with the second hypothesis, we observed a target- and speed-specific bias in the amplitude of responses (Fig. 6c). We compared peak speed and amplitude of calcium responses (peak d*F*/*F* from Gaussian fit) for boutons in the different target areas and found that the boutons in PM tuned to low peak speeds responded more strongly than nearby boutons tuned to high peak speeds (unpaired, two-tailed Student's *t*-test: boutons in PM with a peak speed less than 25 deg s^{-1} versus those with a peak speed more than 100 deg s^{-1}, $P < 10^{-6}$). Conversely, boutons in AL tuned to low speeds showed weaker responses than boutons tuned to high peak speeds ($P < 10^{-7}$). Thus, on average, the response amplitude was larger in the boutons with preferences matched to that of the neurons in the target area.

It is unlikely that the increased response amplitude can be explained by the contribution of out-of-focus fluorescence from neighboring boutons, for two reasons. First, although the distributions of peak speeds for boutons in AL and PM were distinct at all amplitudes (Fig. 6d; K–S tests, AL versus PM: *P*-values $< 10^{-15}$ for all five amplitude ranges tested), the distributions became more distinct as response amplitudes increased (Supplementary Fig. 4a; linear discriminant analysis: the optimal classification accuracy was 70% for boutons with peak d*F*/*F* <0.2 and 92% for boutons with peak d*F*/*F* >1.6). If the effect were due to out-of-focus fluorescence, then one would expect a homogenous increase in d*F*/*F* across the population. Second, this effect was clearest for the most strongly responding boutons (d*F*/*F* >0.8, about 10% of all imaged boutons; Fig. 6e; unpaired, two-tailed Student's *t*-test: comparison of average peak speed of weakly (d*F*/*F* <0.4) versus strongly (d*F*/*F* >0.8) responding boutons in AL and PM: all *P*-values $< 10^{-6}$). However, the neuropil response

was an order of magnitude weaker than that of the strongly responding boutons (average peak neuropil response, 0.08; range across all fields of view, 0.04–0.16; see Online Methods) and therefore cannot account for these responses. Thus, our data demonstrate specificity in both the density (Fig. 5) and the response amplitude (Fig. 6) of functionally matched V1 projection boutons in a given target area.

Functional specificity of LM projections

We next addressed whether the target specificity we observed in projections from V1 may be a general rule for feed-forward visual cortical projections. Like cell bodies in V1, those in the secondary visual area LM have diverse receptive fields[5,25] and project directly to areas AL and PM[24]. This led us to investigate whether the targets of area LM also receive target-specific sensory input.

We made small, targeted injections of a viral vector carrying GCaMP3 so that expression was contained within the borders of LM (Fig. 7a and Supplementary Fig. 5). The densest projections from LM were found in areas AL, PM and AM (anteromedial; Fig. 7a; we also observed a diffuse feedback projection in area V1 (ref. 24)). We focused on areas AL and PM to directly compare the projections from LM with the convergent projections from V1. Wide-field epifluorescence microscopy revealed bright islands of labeled axons (Supplementary Fig. 5d), which we then targeted for two-photon imaging in a manner identical to that described above for projections from V1 (average depth, 98.7 μm; range, 50–150 μm below the pia; 12 fields of view; six mice).

We measured spatial and temporal frequency tuning for LM axonal boutons in areas AL (1,673 boutons, four mice, six fields of view) and PM (910 boutons, five mice, six fields of view). Although some diversity was evident among nearby boutons in the same field of view (Fig. 7b), the average tuning of projections from LM to areas AL and PM was distinct (Fig. 7c,d). LM projections to AL responded more strongly to lower spatial and higher temporal frequencies (Fig. 7d,e; paired, two-tailed Student's t-test, comparison of dF/F in response to high versus low spatial or temporal frequencies: all P-values $< 10^{-50}$), whereas LM projections to PM responded more strongly to higher spatial frequencies ($P < 0.001$) but had no temporal frequency preference ($P > 0.5$). Thus, projections from LM to AL responded more strongly to high speeds ($P < 10^{-50}$), whereas those to PM did not prefer high over low speeds ($P > 0.05$). Moreover, the average tuning of projections to AL was distinct from those to PM (Fig. 7d) and was more correlated across experiments within an area than across areas (correlation coefficient within an area, 0.38 ± 0.08, $n = 18$ pairs, five mice; across areas, -0.08 ± 0.13, $n = 9$ pairs; unpaired, two-tailed Student's t-test: $P < 0.05$).

The distributions of spatial and temporal frequency preferences of boutons from LM in AL and PM were also distinct (Fig. 7f,g; K–S tests, AL versus PM: all P-values $< 10^{-13}$ for spatial and temporal frequency and speed). The projections from LM to AL and PM had area-specific biases qualitatively similar to, albeit smaller than, those seen in the projections from V1. The most notable difference between projections from LM and V1 was the greater proportion of LM boutons preferring high temporal frequencies, which was likely due to the higher temporal frequency preference of cell bodies in LM relative to those in V1 (refs. 4,5,25).

We thus found that the downstream targets of LM, like those of V1, each received distinct visual information. Moreover, projections from LM generally matched the functional preferences of the projections from V1, as well as the functional preferences of neurons in each target area.

DISCUSSION

We used two-photon calcium imaging to examine whether higher visual areas receive functionally specific projections from V1 by measuring the visual response properties—the tuning for spatial and temporal frequency—of V1 axons projecting to three downstream visual areas: LM, AL and PM. We found that all three projections, as measured by the response properties of individual presynaptic boutons, were functionally distinct and were, moreover, matched to the function of the neurons in each target area. Therefore, the population of neurons in V1 makes functionally target-specific projections. These data suggest that functionally specific connections are important in determining the specialization of receptive field preferences of neurons in the higher visual areas.

Functional imaging of projections in mouse visual cortex

The ability to characterize projections to multiple areas was made possible largely by the simplicity of our imaging-based approach: the origin of each axon was determined by the site of the viral injection, and its target was determined by the imaging site[29,30]. By contrast, most previous studies that addressed target specificity have used antidromic stimulation to identify the projection target[19,20,31,32], which requires great care to avoid false positives and negatives[33]. Instead, we were able to survey the tuning properties of hundreds of boutons from the same mice and compare several projection pathways with our functional imaging approach. Because synaptic boutons represent fundamental units of synaptic transmission, their numbers and response amplitudes reflect the net impacts of these inputs on their targets. Thus, such direct comparisons constitute an important step toward generating a functional projectome—a model of the transmission of information between each cortical area.

We found that each of the higher visual areas received distinct functional information from V1. This was true when looking at both the average tuning (Fig. 2) and the diversity of peak preferences (Fig. 5) and is consistent with the segregation of cortico-cortical projection neurons into discrete anatomical (refs. 32,34 and Q. Wang & A. Burkhalter, *Soc. Neurosci. Abstr.* 854.1, 2005) and functional[21,22] streams. Despite being a common feature of systems with functionally segregated architecture[11–13,15,16,19], we have found that such segregation can arise from a locally diverse neuronal population (Figs. 3 and 4).

The functional match between feed-forward projections and their target neurons could account for the increase in specificity seen in the higher visual areas. Nonetheless, additional mechanisms, such as target-specific thalamic inputs[35] or local processing within the higher visual areas[36], could also contribute to the specialization.

Mechanisms of target specificity in mouse visual cortex

We found a different distribution of stimulus preferences for boutons in each area. This could be due to either an increased probability of projection or a larger axonal arborization of V1 neurons that are functionally matched to the target area. Both models result in the selective transmission of information to the higher visual areas; our approach does not distinguish between them. Complementary approaches such as retrograde labeling of projection neurons give a more direct measurement of projection probability[21,22]. In fact, one such study found comparatively weak differences in the spatial and temporal frequency preferences of neurons projecting to different higher visual areas in the ferret[22], suggesting that the density of the axonal arborizations may be an important factor in determining the target specificity of projections.

Both models can potentially be explained by target-specific refinement of axonal projections. Feed-forward projections arborize well before eye-opening (as early as postnatal

day 2), but the density of these arborizations continues to increase over the first month of life[34,37]. This is consistent with the initial targeting of the higher visual areas being genetically determined (potentially by means of molecular signals expressed by distinct groups of cortical neurons[38]), followed by refinement through experience-dependent plasticity[39]. Nonetheless, our data suggest that this must be regulated at the level of individual neurons (Fig. 3).

We also found that projections with preferences matched to their target area had larger amplitude responses. This larger change in indicator fluorescence may be due to these neurons firing more action potentials. Such an effect could be mediated through amplification of signals by preferentially connected subnetworks within V1 (refs. 9,10,40–43). Alternatively, the amplitude of responses may depend more on the properties of individual boutons: larger boutons may have a greater calcium channel density or number of active zones, resulting in more calcium influx per action potential[27]. In this case, the increased response amplitude may reflect a higher probability of release and could be the result of synapse-specific Hebbian plasticity[44,45].

Although we found differences in both the density and response amplitude of target-specific projections to AL and PM, these two measurements may not be completely independent. The increase in density may result in the grouping of more than one bouton into the same region of interest, thereby increasing the measured response amplitude. However, the sparseness of responsive boutons and the weak relationship between baseline fluorescence and dF/F (Supplementary Fig. 4b) both provide evidence against this possibility. Conversely, the greater response amplitude could bias selection of boutons and therefore inflate bouton counts. However, this is likely to have only a minor influence, as distributions of bouton densities were consistent for each of the lower ranges of response amplitudes (Fig. 6d). In addition, because the strongly responding boutons are such a small percentage of the population, we expect that the difference in bouton density dominates in generating the target specificity.

The transmission of information throughout visual cortex

Owing to its position in the visual cortical circuit and its diversity of responses, V1 acts as a hub for transmitting several information channels from a locally heterogeneous population. Thus, local circuitry within V1, including recurrent excitation within networks and nonspecific inhibition across networks[10,46,47], is likely important in shaping the content of these streams. In addition, any modulation of activity in V1, such as the changes in excitability and shifts in tuning that occur during locomotion[4,48], could affect the flow of information through the cortex.

Axonal projections exclusively from layer 5 and from the secondary visual area LM also made target-specific projections to the higher visual areas (Figs. 4 and 7), suggesting that the segregation of diverse sensory information may be a general feature of mouse visual cortex. This finding provides a context for the widespread connectivity that has been found between the areas of the visual system[49,50]. The projectome of the visual cortical areas (the graph of inter-areal projections) is virtually all-to-all in the mouse, although there is a clear substructure when the weights of connections are considered[49]. Here we have found that, rather than sending duplicated information to different areas across the brain, each projection likely transmits distinct sensory information tailored to its target. By revealing the specific rules that govern organization of these projections at the cellular and functional level—the functional projectome—we can begin to predict how the specific transmission of visual information can guide task-dependent visual behaviors.

ONLINE METHODS

Mice

All procedures were conducted in accordance with the ethical guidelines of the NIH and approved by the IACUC at Harvard Medical School. Twenty-four mice (both sexes; 3–12 months old; C57BL/6 was the primary background (up to 50% Balb/C); singly housed on a reverse light-dark cycle) were used in this study; this number of mice was required to have sufficient data from multiple lines and injection sites (see below). Selective labeling of layer 5 neurons was achieved by using the Rbp4-KL100 BAC-cre driver line[51] (MMRRC no. 031125-UCD); crosses with Rosa-CAG-LSL-tdTomato-WPRE:: deltaNeo line[52] (Jax no. 007914) enabled visualization of expression (Fig. 4a).

Cranial window implant and habituation

Dexamethasone (3.2 mg/kg, i.m.) was administered at least 2 h before surgery. Animals were anesthetized with ketamine (200 mg/kg, i.p.), xylazine (30 mg/kg, i.p.) and isoflurane (1.2–2% in 100% O_2) and given atropine (0.2 mg/kg, i.p.) at surgery onset. Using aseptic technique, a headpost was secured using cyanoacrylate glue, dental acrylic and C&B Metabond (Parkell), and a 5 mm craniotomy was made over the left hemisphere (center: 2.8 mm lateral, 0.5 mm anterior to lambda)[4] allowing implantation of a glass window (consisting of an 8-mm coverslip bonded to two 5-mm coverslips (Warner no. 1; total thickness: 0.5 mm; thickness below skull: ~200 μm) with refractive index–matched adhesive (Norland no. 71)) using cyanoacrylate glue and dental acrylic. The mice were allowed to recover for at least 4 d.

Habituation consisted of delivering water only during and immediately after head restraint training. Duration of head restraint increased over 1–2 weeks, from 3 min to 2 h. During habituation and imaging, mice were placed on a 6-inch-diameter foam ball (Plasteel) that could spin noiselessly on ball bearings (McMaster-Carr). We monitored trackball revolutions using a custom photodetector circuit. Imaging sessions were 2–4 h in duration.

Targeted expression of calcium indicator

We targeted either V1 or LM (using retinotopic maps; see below) for expression of the calcium indicator GCaMP3.3. Dexamethasone was administered at least 2 h before coverslip removal. Mice were anesthetized (isoflurane, 1–1.5%), the cranial window was sterilized with alcohol and the coverslip removed. We then used a volume injection system (50–100 nl/min, Stoelting) to inject 30–100 nl of a 10:1 mixture of either AAV2/1.hSynap. GCaMP3.SV40 or AAV2/1.hSynap.Flex.GCaMP3.WPRE.SV40 (Penn Vector Core[53]) and sulforhodamine-101 (1 mM; Invitrogen) to visualize the injection. Using the blood vessel pattern as a guide, we made an injection either in the posteromedial part of area V1 (temporal/superior visual field; which provided maximal spatial separation of axonal projections to higher visual areas[23]) or in the same retinotopic representation in area LM, at a depth of 200–300 μm below the pial surface. After the injection, a new cranial window was sealed in place.

Experiments were conducted 2–8 weeks after injection. All mice were imaged using wide-field epifluorescence microscopy to confirm that cell body expression was restricted to the target visual area (V1 or LM; Supplementary Figs. 1 and 5). Retrogradely infected cell bodies were never observed when imaging in LM, AL or PM; on one occasion an infected cell body was seen in layer 2/3 of RL. On several occasions, when viral injections were made into LM, infected cell bodies were seen in superficial layers of V1. The feed-forward projection from V1 to LM is most dense[23] and therefore may be more susceptible to retrograde infection.

Visual stimulation

To achieve precise stimulation at temporal frequencies of 1–15 Hz, we used a 120-Hz LCD monitor (Samsung 2233RZ, 2200) calibrated (at each temporal frequency) using a spectrophotometer[4] (Photo Research PR-650). Waveforms were also confirmed to be sinusoidal by measuring luminance fluctuations of a full-field sinusoidally modulated stimulus (using a photomultiplier tube, Hamamatsu). The monitor was positioned 21 cm from the contralateral eye. Circular 40° patches containing either square-wave (for mapping retinotopy with wide-field imaging of intrinsic autofluorescence or GCaMP3) or sine-wave (for mapping receptive fields with two-photon imaging) drifting gratings (80% contrast with contrast modulated sinusoidally to 0% over the outer 10°) were alternated with periods of uniform mean luminance (59 cd/m^2). Stimuli were centered at monocular locations that most effectively drove axonal responses (45 to 115° azimuth and −5 to 25° elevation; 0° reference is straight ahead (azimuth) and eye-level (elevation)). For characterization of the temporal and spatial frequency tuning of axons, we presented either upward or upward and downward drifting gratings at five spatial frequencies (0.02, 0.04, 0.08, 0.16 and 0.32 c.p.d.) and five temporal frequencies (1, 2, 4, 8 and 15 Hz) for a total of 25 or 50 stimulus types plus 10% blank trials. All stimuli in a set were presented in a randomized order (sampling without replacement) 9–12 times, for 5 s with 5 s of mean luminance between trials. For analysis of spatial and temporal frequency tuning, we combined responses to upwards- and downwards-drifting stimuli.

Wide-field imaging

To map the boundaries of visual cortical areas, we measured changes in the intrinsic autofluorescence signal using epifluorescence imaging[54] (see Supplementary Figs. 1 and 5). Autofluorescence produced by blue excitation (470 ± 40 nm band, Chroma) was measured through a green and red emission filter (longpass, 500 nm cutoff). Images were collected using a CCD camera (Sensicam, Cooke, 344 × 260 pixels spanning 4 × 3 mm; 2 Hz acquisition rate) through a 5× air immersion objective (0.14 numerical aperture (NA), Mitutoyo) using ImageJ acquisition software. For retinotopic mapping, we stimulated at six retinotopic positions (with drifting gratings at 2 Hz and 0.04 c.p.d.) for 10 s each, with 10 s of mean luminance preceding each trial. The response to a stimulus was computed as the fractional change in fluorescence (dF/F) between the average of all frames from 0–3 s (as baseline) and 12–19 s (as response) after stimulus onset. For wide-field imaging of GCaMP3, an identical procedure was used except (i) light was collected with a bandpass filter (525 ± 50 nm), (ii) total trial duration was reduced to 10 s, and (iii) changes in fluorescence were calculated as the dF/F from the 5 s before (as baseline) and 5 s after (as response) stimulus onset.

Two-photon calcium imaging

Imaging was performed with a custom-designed two-photon laser-scanning microscope[8]. Excitation light (920 nm) from a Mai Tai HP DeepSee laser (Newport) was directed into a modulator (Conoptics) and a beam expander (Edmund Optics). The beam was raster scanned onto the brain with a resonant galvanometer (4 kHz, Electro-Optical Products). For axon imaging we used a 0.8 NA, 16× objective (Nikon; power at the sample: 20–45 mW); we used this lower NA objective to increase our depth of field and thereby decrease the effects of z-motion. The imaged field of view was 200–300 μm on a side at resolution of 0.8–1.2 μm per pixel (dwell-time, ~0.3 μs). For cell body imaging, we used a 1.05 NA, 25× objective (Olympus) attached to a piezo z-scanner (P-721.LLQ, Physik Instrumente) to generate a volume at 1 Hz (350–425 μm on a side; 100 μm thick; a total of 31 planes separated by 3 μm). Laser power (10–90 mW) was continuously modulated to account for changes in depth.

Emitted photons were directed through a green filter (center: 542 nm; band: 50 nm; Semrock) onto GaAsP photomultipliers (no cooling, H10770PA-40, Hamamatsu). The photomultiplier signals were amplified (DHPCA-100, Femto) and low-pass filtered (cutoff frequency, ~700 kHz), and images were reconstructed in MATLAB. Microscope control was also performed in MATLAB.

Viral expression of GCaMP3 permitted recording from multiple cortical areas in the same mice on different days. Axons were confirmed to be within a particular cortical area by comparison of the surface vasculature from wide-field imaging (Supplementary Figs. 1 and 5). In the case that the same area in a mouse was targeted for multiple imaging sessions, we located the initial imaging site using vascular markers and imaged either a different depth or an adjacent plane to ensure that all boutons in the sample were unique.

Histology

For *post hoc* histological analysis, mice were perfused with 10 ml 0.1 mM PBS followed by 40 ml of either 4% (for coronal sections) or 2% (for tangential sections) paraformaldehyde (PFA) in PBS. For coronal sections, the whole brain was removed and submerged in 4% PFA overnight. For tangential sections, the injected hemisphere was isolated and the subcortical tissue removed; the cortex was then flattened under a small weight for 4 h in 2% PFA and then submerged in 4% PFA overnight. For both preparations, the brain was then submerged in 30% sucrose in PBS for 24–48 h and sectioned at 50 μm thickness on a freezing microtome. A subset of sections was stained with DAPI (2 μM) before mounting on a gelatinized glass slide. Images were then taken on either an Olympus BX61 with a 4× objective, an Olympus VS110 slide-scanner with 10× objective, or the custom two-photon microscope with a 16× objective.

Data analysis and statistics

Data analyses were performed using MATLAB (MathWorks) and ImageJ (NIH). For bouton imaging, the image stack was registered to the average field of view using sub-pixel registration methods[8] to correct for motion along the imaged plane (x–y motion). A 5-pixel border at each edge of the field of view was removed to eliminate registration artifacts. After registration, all experiments were temporally averaged so that the effective imaging rate was 2.67 Hz. Evoked responses were measured for each stimulus type as the dF/F between the 2.5 s before (baseline) and the 5 s after (as response) stimulus onset, and averaged across trials.

To identify all significantly responsive boutons in the field of view, we performed a three-stage analysis:

First, to identify potential boutons, we identified local maxima, or 'hotspots'. As synaptic boutons are likely to be the strongest local signals in our field of view (owing to their larger volume and calcium channel density[27,28]), regions of interest were chosen from the maximum value of the dF/F signal in response to all stimulus types (max dF/F; see Fig. 1 and Supplementary Fig. 3a). For the selection these local maxima, but not subsequent analyses, the average fluorescence of each frame was subtracted before computing the dF/F (to decrease the effects of global changes in fluorescence) and then smoothed by half a pixel (to limit the identification of spurious maxima). From the resulting dF/F image, we identified all 'hotspots' (that is, pixels that were brighter than all immediate neighbors) as potential boutons.

Second, to select the visually responsive 'hotspots', we calculated the time course for every pixel in the image, averaged with its immediate neighbors (yielding the time course for every 3×3 pixel square). For each of these time courses, we tested whether it was

significantly driven by at least one visual stimulus condition (paired, one-tailed Student's *t*-test), thus generating a map of significance levels. We increased the stringency of our statistical test by first smoothing this map by half a pixel and then applying a threshold (*P* < 0.002, or 0.05/25, to correct for the number of conditions) to create a mask (see Supplementary Fig. 3b).

Finally, we considered only those potential boutons (found in stage 1) that were contained within this mask (found in stage 2) for further analysis (significantly responsive boutons; see Supplementary Fig. 3c). We identified 13,371 significantly responsive boutons from V1 neurons (WT: 3,112 boutons in LM, 5,619 in PM and 2,595 in AL; Rpb4-cre: 922 in LM, 1,006 in PM and 117 in AL) and 3,311 significantly responsive boutons from LM neurons (1,265 boutons in PM and 2,046 in AL).

Most boutons found in this way likely correspond to anatomical presynaptic boutons. First, in many cases the identified boutons could be seen as local maxima in baseline fluorescence images, suggesting that they correspond to synaptic swellings (Supplementary Fig. 2f). Second, examination of the distance between boutons on the same axon (see Fig. 1d) is consistent with inter-synapse distances previously described[55] (~5 μm).

The response of each bouton across all spatial and temporal frequencies was then fit by a two-dimensional elliptical Gaussian[4]:

$$R(sf, tf) = A \exp\left(\frac{-(\log_2 sf - \log_2 sf_0)^2}{2(\sigma_{sf})^2}\right) \cdot \exp\left(\frac{-(\log_2 tf - \log_2 tf_p(sf))^2}{2(\sigma_{tf})^2}\right)$$

where A is the neuron's peak response amplitude, sf_0 and tf_0 are the neuron's preferred spatial and temporal frequencies, and σ_{sf} and σ_{tf} are the spatial and temporal frequency tuning widths. The dependence of temporal frequency preference on spatial frequency is captured by a power-law exponent ξ, such that

$$\log_2(tf_p(sf)) = \xi(\log_2 sf - \log_2 sf_0) + \log_2 tf_0$$

For this protocol, we estimated upper and lower confidence bounds for sf_0 and tf_0 by performing 500 Monte-Carlo simulations (random sampling of trials of each stimulus type with replacement). Only boutons with 95% confidence intervals less than 2 octaves for both sf_0 and tf_0 were included in subsequent analyses. This strict criterion eliminated ~30% of the boutons from V1 neurons (30% of boutons in LM, 31% in PM and 29% in AL), leaving 9,290 significantly responsive, well-fit boutons in all areas (WT: 2,252 boutons in LM, 3,931 in PM and 1,902 in AL; Rbp4-cre: 559 in LM, 618 in PM and 28 in AL). A similar proportion of the boutons from LM were also eliminated in this way (28% of boutons in PM and 18% of boutons in AL), leaving 2,583 significantly responsive, well-fit boutons (910 boutons in PM and 1,673 in AL). All significantly responsive, well-fit boutons were considered when determining the average tuning and distribution of bouton preferences in each area. However, when addressing the average tuning of all boutons imaged within a mouse (Figs. 2c bottom, 5c, 7d bottom and 7g), only those areas with at least 25 significantly responsive, well-fit boutons were considered for analysis.

Notably, all of the steps involved in selection of boutons were automated, thereby reducing the possibility for experimental bias. Moreover, the difference in preferences between areas was not dependent on the selection or fitting of boutons. Area-specific differences in the

tuning of boutons in AL and PM were maintained when considering (i) all pixels, (ii) all significantly responsive pixels or (iii) all boutons in each field of view (Supplementary Fig. 3; paired, two-tailed Student's t-test comparing the three lowest versus three highest speeds: all P-values $< 10^{-50}$).

In each field of view, only a small percentage of the total pixels were identified as boutons (average across all fields of view: 3%). The sparse axonal activation was not due to sparse anatomical innervation, as there were many bright pixels in the baseline image that were not visually driven (Supplementary Fig. 2f). Instead, it was probably due to sparse activity of cell bodies in V1, owing to the incomplete mapping of visual stimulus space and to sublinear GCaMP3 responses at low firing rates.

Despite the sparseness of responses, out-of-focus fluorescence ('neuropil' response) may contaminate bouton responses. To estimate the neuropil contribution, we averaged the response from all pixels in the field of view except those belonging to expanded bouton masks (a 5×5 pixel square surrounding each bouton). This procedure for estimating the neuropil response may be contaminated by visually evoked in-plane fluorescence from (i) boutons that did not pass our requirements for inclusion or (ii) intervening axonal segments, and therefore is an overestimate of the out-of-focus fluorescence contamination. Nonetheless, we found the average peak neuropil response to be 0.08 (range across all fields of view: 0.04–0.16), and therefore it should minimally contaminate most boutons (70% of boutons have a dF/F > 0.2; see Fig. 6d). Moreover, when looking at individual boutons (Fig. 1e and Supplementary Fig. 2e), we do not see neuropil responses to nonpreferred stimuli; nor are there strong correlations across all boutons in the same field of view (Supplementary Fig. 2b).

For cell body imaging, imaging volumes were aligned volume-by-volume to correct for slow drifts and x–y motion[56]. Three-dimensional cell masks were obtained by taking the maximal dF/F for all stimulus types (the same time windows were used as for boutons) and using custom, semiautomated segmentation algorithms. Fluorescence time courses were generated by averaging all pixels in a cell mask. Neuropil signals were removed by first selecting a spherical shell around each neuron (excluding neighboring neurons), estimating the common time course of all shells in the volume (first principal component) and removing this component from each cell's time course (scaled by the baseline fluorescence of the surrounding shell)[4]. For each cell, we tested whether it was significantly driven by at least one visual stimulus condition and could be well-fit by a two-dimensional elliptical Gaussian (same requirements as for boutons). There were 943 neurons (in WT and RBP4-cre mice) that were initially segmented; of these, 779 were significantly responsive and 701 were well-fit.

Cellular depth was determined by finding the centroid of each cellular mask and aligning each imaged volume to a larger reference stack for that mouse (450 μm on a side; from the pia through layer 5 in 2-μm steps). The reference stack was corrected for tilt by rotating the volume so that the pia was horizontal; the beginning of layer 4 was determined by the sharp decrease in cellular density (likely due to the tropism of the AAV); the beginning of layer 5 was determined by the marked increase in cellular size. Laminar borders were confirmed with *post hoc* DAPI staining (Fig. 3a).

Tuning distance was calculated, using speed preferences for pairs of cells, as

$$Tuning\ distance = \frac{|[\log_2(Speed_{cell1}) - \log_2(Speed_{cell2})]|}{[\log_2(Speed_{max}) - \log_2(Speed_{min})]}$$

such that the maximal tuning distance is 1.

Despite the nonlinear relationship between spiking and GCaMP3 fluorescence[53], the peak responses used to estimate spatial and temporal frequency preferences (Figs. 3–7) should be insensitive to this nonlinearity and reflect the peak spiking response[4]. Although the supra-linear relationship between number of spikes and increase in fluorescence[53] may inflate the measured response amplitude of the strongest responding boutons, there is nonetheless a selective increase in the response of a subset of target-specific boutons (Fig. 6). Further, the increased responses of boutons at high speeds in AL but at low speeds in PM make it unlikely that the bias in response amplitude is due to a systematic interaction of stimulus properties and the nonlinearity of the calcium indicator.

All data are given in mean ± s.e.m. Differences in dF/F and tuning within and across areas were tested for significance using a Student's t-test (pairing and number of tails chosen according to experiment). In cases where a nonparametric test was appropriate, a Wilcoxon rank-sum or a Kolmolgorov-Smirnov test was used.

Supplementary Material

Refer to Web version on PubMed Central for supplementary material.

Acknowledgments

References

1. Dräger UC. Receptive fields of single cells and topography in mouse visual cortex. J Comp Neurol. 1975; 160:269–290. [PubMed: 1112925]

2. Niell CM, Stryker MP. Highly selective receptive fields in mouse visual cortex. J Neurosci. 2008; 28:7520–7536. [PubMed: 18650330]

3. Gao E, DeAngelis GC, Burkhalter A. Parallel input channels to mouse primary visual cortex. J Neurosci. 2010; 30:5912–5926. [PubMed: 20427651]

4. Andermann ML, Kerlin AM, Roumis DK, Glickfeld LL, Reid RC. Functional specialization of mouse higher visual cortical areas. Neuron. 2011; 72:1025–1039. [PubMed: 22196337]

5. Marshel JH, Garrett ME, Nauhaus I, Callaway EM. Functional specialization of seven mouse visual cortical areas. Neuron. 2011; 72:1040–1054. [PubMed: 22196338]

6. Roth MM, Helmchen F, Kampa BM. Distinct functional properties of primary and posteromedial visual area of mouse neocortex. J Neurosci. 2012; 32:9716–9726. [PubMed: 22787057]

7. Ohki K, Chung S, Ch'ng YH, Kara P, Reid RC. Functional imaging with cellular resolution reveals precise micro-architecture in visual cortex. Nature. 2005; 433:597–603. [PubMed: 15660108]

8. Bonin V, Histed MH, Yurgenson S, Reid RC. Local diversity and fine-scale organization of receptive fields in mouse visual cortex. J Neurosci. 2011; 31:18506–18521. [PubMed: 22171051]

9. Ohki K, Reid RC. Specificity and randomness in the visual cortex. Curr Opin Neurobiol. 2007; 17:401–407. [PubMed: 17720489]

10. Ko H, et al. Functional specificity of local synaptic connections in neocortical networks. Nature. 2011; 473:87–91. [PubMed: 21478872]

11. Livingstone MS, Hubel DH. Specificity of cortico-cortical connections in monkey visual system. Nature. 1983; 304:531–534. [PubMed: 6308468]

12. DeYoe EA, Van Essen DC. Segregation of efferent connections and receptive field properties in visual area V2 of the macaque. Nature. 1985; 317:58–61. [PubMed: 2412132]

13. Livingstone MS, Hubel DH. Connections cytochrome between layer 4B of area 17 and the thick oxidase stripes of area 18 in the squirrel monkey. J Neurosci. 1987; 7:3371–3377. [PubMed: 2824713]

14. Shipp S, Zeki S. The organization of connections between areas V5 and V2 in macaque monkey visual cortex. Eur J Neurosci. 1989; 1:333–354. [PubMed: 12106143]

15. Sincich LC, Horton JC. Independent projection streams from macaque striate cortex to the second visual area and middle temporal area. J Neurosci. 2003; 23:5684–5692. [PubMed: 12843271]

16. Nassi JJ, Callaway EM. Specialized circuits from primary visual cortex to V2 and area MT. Neuron. 2007; 55:799–808. [PubMed: 17785186]

17. Nassi JJ, Callaway EM. Parallel processing strategies of the primate visual system. Nat Rev Neurosci. 2009; 10:360–372. [PubMed: 19352403]

18. Johnson RR, Burkhalter A. A polysynaptic feedback circuit in rat visual cortex. J Neurosci. 1997; 17:7129–7140. [PubMed: 9278547]

19. Movshon JA, Newsome WT. Visual response properties of striate cortical neurons projecting to area MT in macaque monkeys. J Neurosci. 1996; 16:7733–7741. [PubMed: 8922429]

20. Ferraina S, Paré M, Wurtz RH. Comparison of cortico-cortical and cortico-collicular signals for the generation of saccadic eye movements. J Neurophysiol. 2002; 87:845–858. [PubMed: 11826051]

21. Sato TR, Svoboda K. The functional properties of barrel cortex neurons projecting to the primary motor cortex. J Neurosci. 2010; 30:4256–4260. [PubMed: 20335461]

22. Jarosiewicz B, Schummers J, Malik WQ, Brown EN, Sur M. Functional biases in visual cortex neurons with identified projections to higher cortical targets. Curr Biol. 2012; 22:269–277. [PubMed: 22305753]

23. Wang Q, Burkhalter A. Area map of mouse visual cortex. J Comp Neurol. 2007; 502:339–357. [PubMed: 17366604]

24. Wang Q, Gao E, Burkhalter A. Gateways of ventral and dorsal streams in mouse visual cortex. J Neurosci. 2011; 31:1905–1918. [PubMed: 21289200]

25. Van den Bergh G, Zhang B, Arckens L, Chino YM. Receptive-field properties of V1 and V2 neurons in mice and macaque monkeys. J Comp Neurol. 2010; 518:2051–2070. [PubMed: 20394058]

26. Coogan TA, Burkhalter A. Hierarchical organization of areas in rat visual cortex. J Neurosci. 1993; 13:3749–3772. [PubMed: 7690066]

27. Brenowitz SD, Regehr WG. Reliability and heterogeneity of calcium signaling at single presynaptic boutons of cerebellar granule cells. J Neurosci. 2007; 27:7888–7898. [PubMed: 17652580]

28. Dreosti E, Odermatt B, Dorostkar MM, Lagnado L. A genetically encoded reporter of synaptic activity *in vivo*. Nat Methods. 2009; 6:883–889. [PubMed: 19898484]

29. Petreanu L, et al. Activity in motor-sensory projections reveals distributed coding in somatosensation. Nature. 2012; 489:299–303. [PubMed: 22922646]

30. Nikolaou N, et al. Parametric functional maps of visual inputs to the tectum. Neuron. 2012; 76:317–324. [PubMed: 23083735]

31. Churchland AK, Lisberger SG. Discharge properties of MST neurons that project to the frontal pursuit area in macaque monkeys. J Neurophysiol. 2005; 94:1084–1090. [PubMed: 15872067]

32. Swadlow HA, Weyand TG. Efferent systems of the rabbit visual cortex: laminar distribution of the cells of origin, axonal conduction velocities, and identification of axonal branches. J Comp Neurol. 1981; 203:799–822. [PubMed: 6173404]

33. Swadlow HA. Neocortical efferent neurons with very slowly conducting axons: strategies for reliable antidromic identification. J Neurosci Methods. 1998; 79:131–141. [PubMed: 9543479]

34. Berezovskii VK, Nassi JJ, Born RT. Segregation of feedforward and feedback projections in mouse visual cortex. J Comp Neurol. 2011; 519:3672–3683. [PubMed: 21618232]

35. Simmons PA, Lemmon V, Pearlman AL. Afferent and efferent connections of the striate and extrastriate visual cortex of the normal and reeler mouse. J Comp Neurol. 1982; 211:295–308. [PubMed: 7174895]

36. Jia H, Rochefort NL, Chen X, Konnerth A. Dendritic organization of sensory input to cortical neurons *in vivo*. Nature. 2010; 464:1307–1312. [PubMed: 20428163]

37. Dong H, Wang Q, Valkova K, Gonchar Y, Burkhalter A. Experience-dependent development of feedforward and feedback circuits between lower and higher areas of mouse visual cortex. Vision Res. 2004; 44:3389–3400. [PubMed: 15536007]

38. Molyneaux BJ, et al. Novel subtype-specific genes identify distinct subpopulations of callosal projection neurons. J Neurosci. 2009; 29:12343–12354. [PubMed: 19793993]

39. Hata Y, Tsumoto T, Stryker MP. Selective pruning of more active afferents when cat visual cortex is pharmacologically inhibited. Neuron. 1999; 22:375–381. [PubMed: 10069342]

40. Brown SP, Hestrin S. Intracortical circuits of pyramidal neurons reflect their long-range axonal targets. Nature. 2009; 457:1133–1136. [PubMed: 19151698]

41. Morishima M, Kawaguchi Y. Recurrent connection patterns of corticostriatal pyramidal cells in frontal cortex. J Neurosci. 2006; 26:4394–4405. [PubMed: 16624959]

42. Yoshimura Y, Dantzker J, Callaway EM. Excitatory cortical neurons form fine-scale functional networks. Nature. 2005; 433:868–873. [PubMed: 15729343]

43. Bosking WH, Zhang Y, Schofield B, Fitzpatrick D. Orientation selectivity and the arrangement of horizontal connections in tree shrew striate cortex. J Neurosci. 1997; 17:2112–2127. [PubMed: 9045738]

44. Allen CB, Celikel T, Feldman DE. Long-term depression induced by sensory deprivation during cortical map plasticity *in vivo*. Nat Neurosci. 2003; 6:291–299. [PubMed: 12577061]

45. Zhao C, Dreosti E, Lagnado L. Homeostatic synaptic plasticity through changes in presynaptic calcium influx. J Neurosci. 2011; 31:7492–7496. [PubMed: 21593333]

46. Hofer SB, et al. Differential connectivity and response dynamics of excitatory and inhibitory neurons in visual cortex. Nat Neurosci. 2011; 14:1045–1052. [PubMed: 21765421]

47. Bock DD, et al. Network anatomy and *in vivo* physiology of visual cortical neurons. Nature. 2011; 471:177–182. [PubMed: 21390124]

48. Niell CM, Stryker MP. Modulation of visual responses by behavioral state in mouse visual cortex. Neuron. 2010; 65:472–479. [PubMed: 20188652]

49. Wang Q, Sporns O, Burkhalter A. Network analysis of corticocortical connections reveals ventral and dorsal processing streams in mouse visual cortex. J Neurosci. 2012; 32:4386–4399. [PubMed: 22457489]

50. Felleman DJ, Van Essen DC. Distributed hierarchical processing in the primate cerebral cortex. Cereb Cortex. 1991; 1:1–47. [PubMed: 1822724]

51. Gong S, et al. Targeting Cre recombinase to specific neuron populations with bacterial artificial chromosome constructs. J Neurosci. 2007; 27:9817–9823. [PubMed: 17855595]

52. Madisen L, et al. A robust and high-throughput Cre reporting and characterization system for the whole mouse brain. Nat Neurosci. 2010; 13:133–140. [PubMed: 20023653]

53. Tian L, et al. Imaging neural activity in worms, flies and mice with improved GCaMP calcium indicators. Nat Methods. 2009; 6:875–881. [PubMed: 19898485]

54. Husson TR, Mallik AK, Zhang JX, Issa NP. Functional imaging of primary visual cortex using flavoprotein autofluorescence. J Neurosci. 2007; 27:8665–8675. [PubMed: 17687044]

55. Braitenberg, V.; Schüz, A. Anatomy of the Cortex: Statistics and Geometry. Springer; 1991.

56. Kerlin AM, Andermann ML, Berezovskii VK, Reid RC. Broadly tuned response properties of diverse inhibitory neuron subtypes in mouse visual cortex. Neuron. 2010; 67:858–871. [PubMed: 20826316]
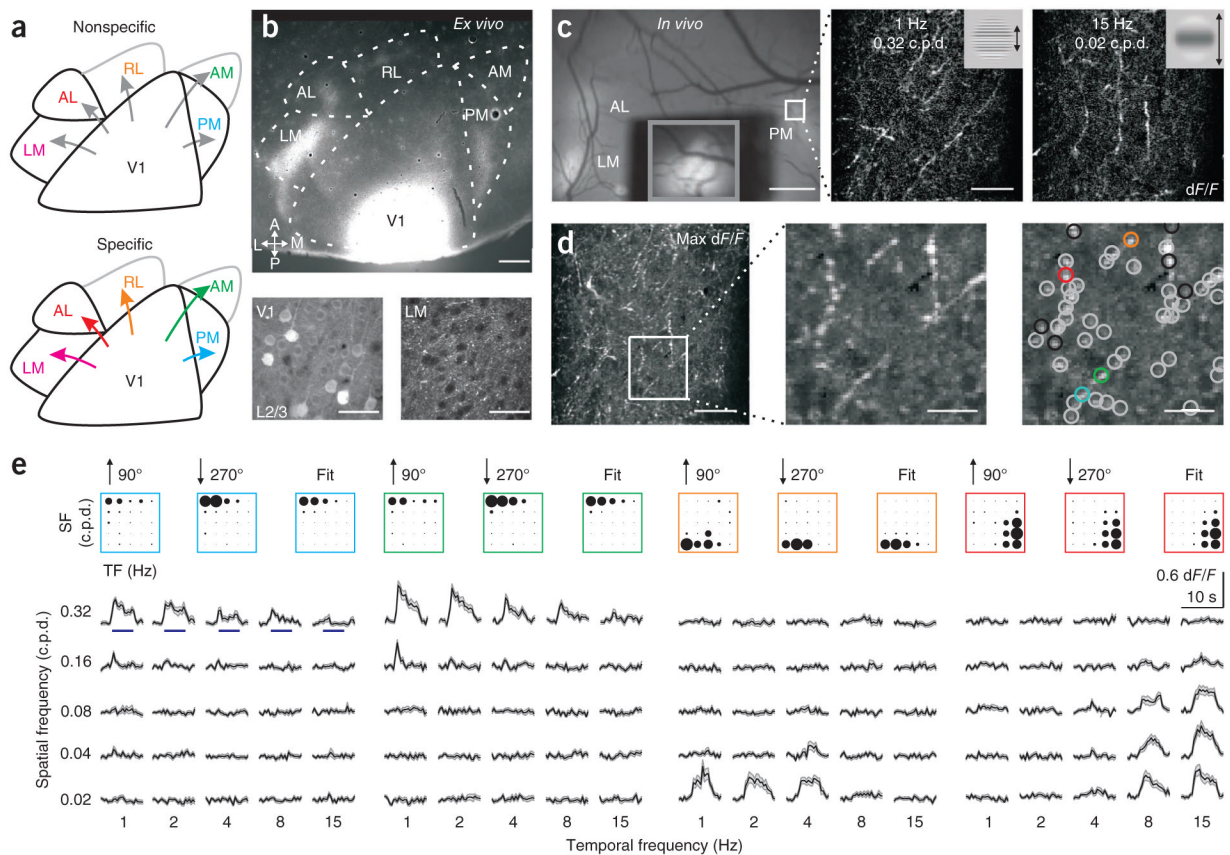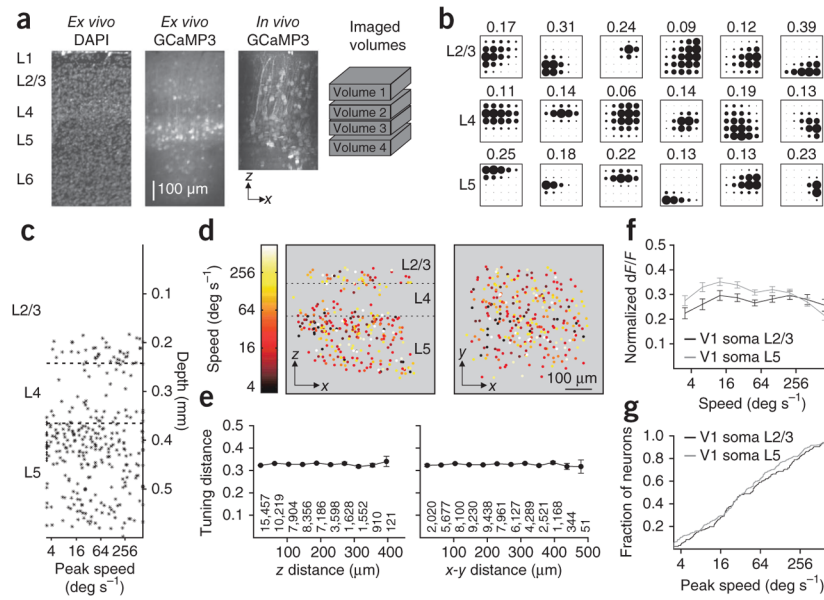
Figure 1.
Functional two-photon calcium imaging from the axons of V1 projection neurons. (**a**) Two models of mouse visual cortex. Higher visual areas may receive functionally nonspecific (top) or specific (bottom) inputs from V1. Specificity may arise through diverse mechanisms, including a bias in projection probability, arborization size or neural excitability. (**b**) Labeling of V1 axonal projections with GCaMP3.3. Top, tangential section of visual cortex; A, anterior; P, posterior; L, lateral; M, medial. Bottom, infected somata in layer 2/3 (L2/3) of V1 (left) and V1 axonal arborizations in LM (right). Scale bars, 500 μm (top) and 30 μm (bottom). (**c**) *In vivo* calcium imaging. Left, *in vivo* image of visual cortex. V1 was covered to prevent saturation and the inset (gray box) taken with lower illumination. Middle and right, example average two-photon fluorescence responses (d*F*/*F*; 24 trials) of axons in PM (white outlined region in left panel). Stimuli (insets) are sinusoidal drifting gratings of different spatial and temporal frequencies. Scale bars, 500 μm (left) and 50 μm (middle and right). (**d**) Identification of visually responsive boutons. Left, maximum (max) response projection across stimuli. Middle, magnification of the boxed region at left. Right, gray and colored circles indicate locations of boutons whose tunings are well fit by a two-dimensional Gaussian. Black circles indicate poor fits (excluded from further analysis). Scale bars, 50 μm (left) and 15 μm (middle and right). (**e**) Visual responses of boutons in colored circles from **d**. Top, average response of each bouton (for the indicated directions of motion; 12 trials per stimulus) and the fit of the average response (right). The area of each circle is proportional to d*F*/*F*. SF, spatial frequency; TF, temporal frequency. Bottom, average d*F*/*F* time course for each stimulus. Blue lines (in left panel) represent duration of stimulus (5 s). Shaded regions are ± s.e.m.
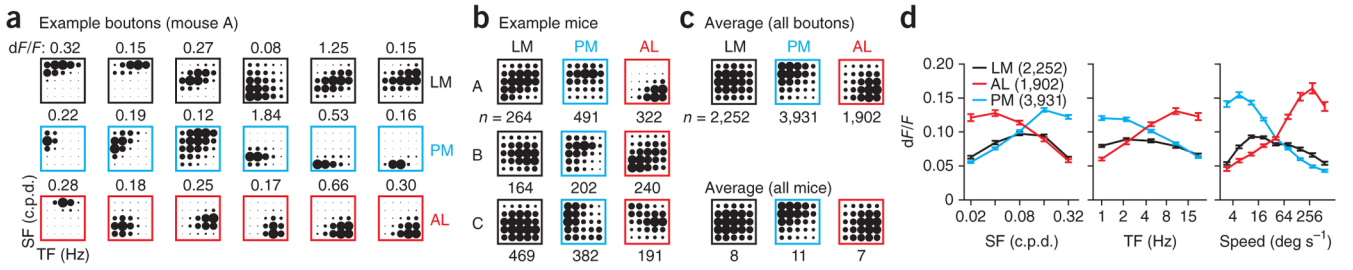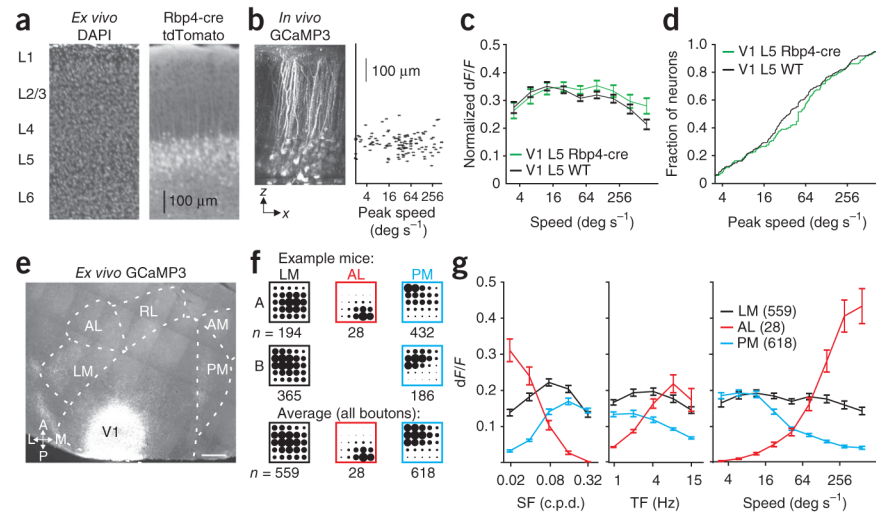
Figure 2.
V1 axons projecting to LM, AL and PM are functionally distinct. (**a**) Example responses from six boutons from the same field of view in LM (top), PM (middle) or AL (bottom) of the same mouse. Boutons were ordered from lowest to highest speed and chosen as evenly spaced percentiles (14th, 29th, 43rd, 57th, 71st and 86th). Amplitude of peak d*F/F* is noted above each response. SF, spatial frequency; TF, temporal frequency. (**b**) Average response of all boutons (*n* represents number of boutons) in LM (left), PM (middle) and AL (right) for three example mice. (**c**) Top, average response in each area for all boutons imaged. Bottom, average response in each area for all mice imaged (*n* represents number of mice). (**d**) Average tuning curves for SF (left), TF (middle) and speed (right) in each area for all boutons imaged. Number of boutons is given in parentheses. Error bars, ± s.e.m.
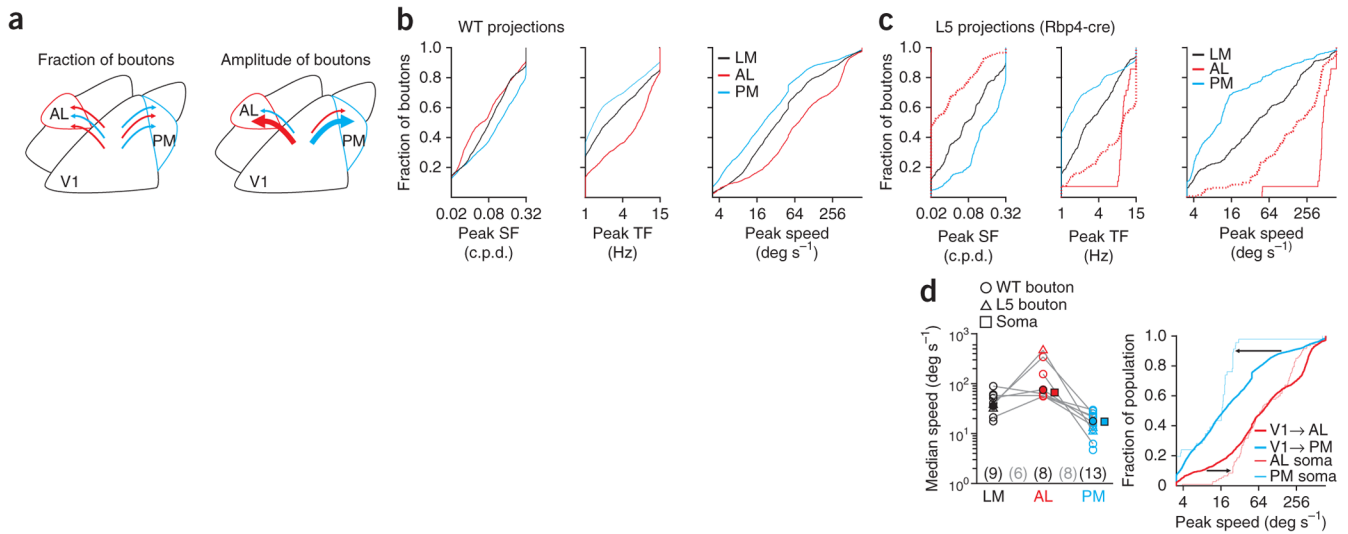
Figure 3.
Lack of functional organization for speed in V1. (**a**) Coronal section of V1 stained with DAPI to show nuclei (left) and expressing GCaMP3 (second from left). Third from left, projection of a *z*-stack taken through the injection site *in vivo* (2-μm steps; same mouse as on left). Right, relative positions of four volumes imaged in this mouse. Layers are indicated at left. (**b**) Example responses from six neurons in L2/3 (top), L4 (middle) or L5 (bottom) from the same mouse as in **a**. Neurons were ordered from lowest to highest speed and chosen as evenly spaced percentiles. Amplitude of peak d*F/F* is noted above each response. (**c**) Scatter plot of peak speed by cortical depth for all neurons (*n* = 302) imaged in the mouse in **a**. Dashed lines delineate the borders of L4. (**d**) *x*–*z* (left) and *x*–*y* (right) projection of all neurons imaged in the mouse in **a**, colored according to peak speed. Note the lack of clustering in any dimension. (**e**) Average tuning distance (see Online Methods) for all pairs of neurons binned according to their distance in *z* (left) and *x*–*y* (right) (*n* = 542 neurons, two mice; the number of pairs for each bin is given below; bins with <10 pairs were excluded). (**f**) Average tuning for speed for neurons in L2/3 (*n* = 166 neurons, four mice) and L5 (*n* = 312 neurons, two mice). (**g**) Cumulative distribution of peak speeds for neurons in L2/3 and L5 (same population of neurons as in **f**). All error bars, ± s.e.m.
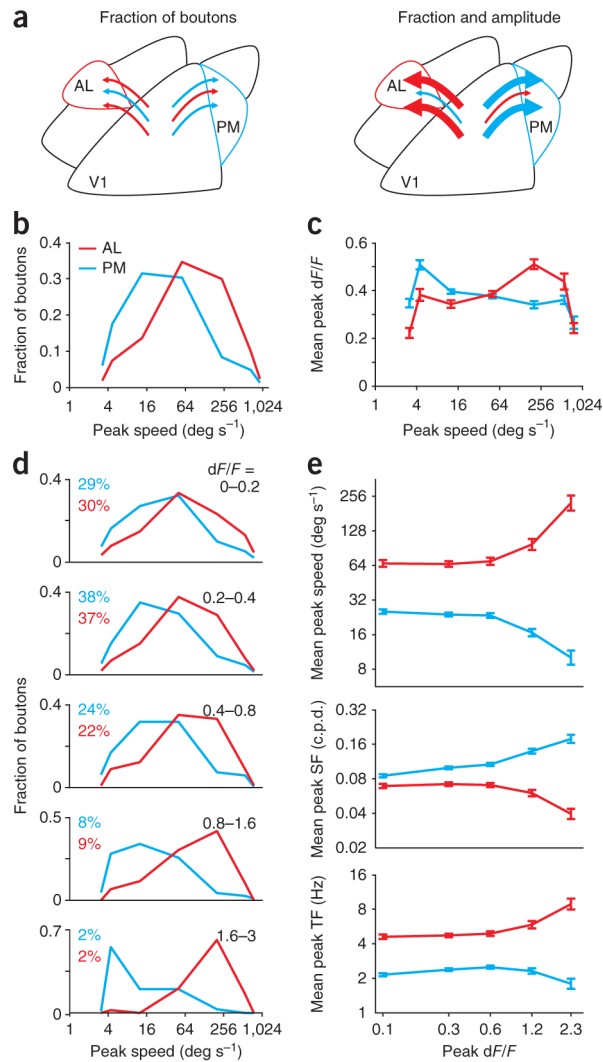
Figure 4.

Layer 5 axons projecting to LM, AL and PM are functionally distinct. (**a**) Coronal section of visual cortex stained for DAPI (left) from an Rbp4-cre × tdTomato reporter (right) mouse. Note the dense expression in layer 5 (L5). (**b**) Left, *x–z* projection of an *in vivo z*-stack of an Rbp4-cre mouse after infection with GCaMP3 (2-μm steps). Right, scatter plot of peak speed by cortical depth for all neurons imaged ($n = 121$) in the mouse on left. (**c**) Average tuning for speed for neurons in L5 of WT ($n = 312$ neurons, two mice) and Rbp4-cre mice ($n = 159$ neurons, two mice). (**d**) Cumulative distribution of peak speeds for neurons in L5 of WT and Rbp4-cre (same population of neurons as in **c**). (**e**) Tangential section of visual cortex of an Rbp4-cre mouse (same mouse as in **b**) after infection with GCaMP3. Scale bar, 500 μm; abbreviations as in Figure 1. (**f**) Average response of all boutons (*n* represents number of boutons) in LM (left), AL (middle) and PM (right) for two example mice (top and middle) and for all boutons imaged in each area (bottom). (**g**) Average tuning curves for spatial frequency (SF; left), temporal frequency (TF; middle) and speed (right) for all boutons imaged in each area. All error bars, ± s.e.m.
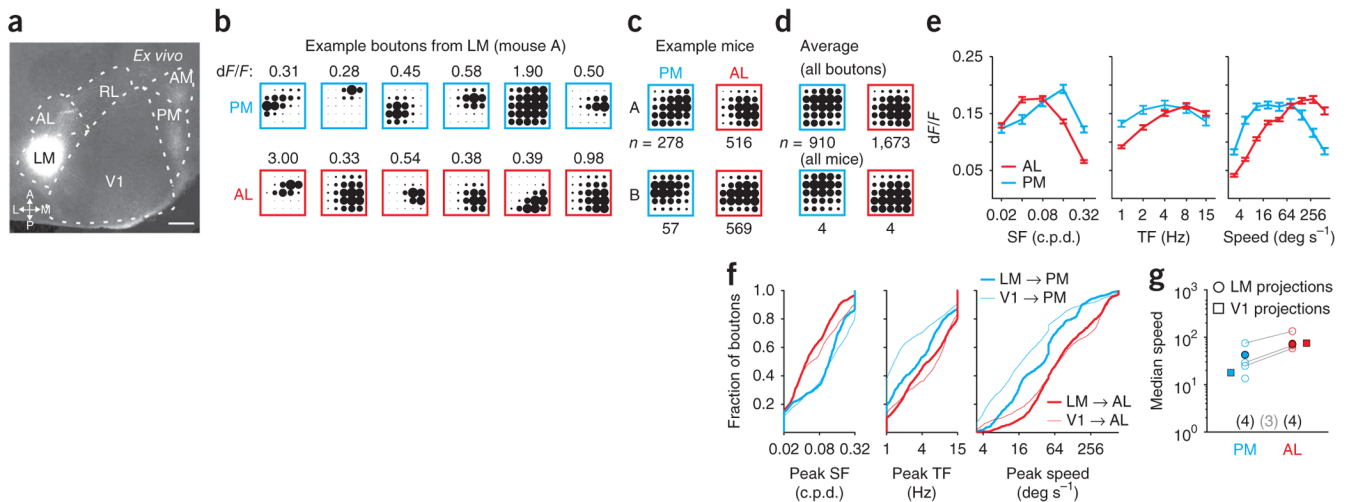
Figure 5.
Bias in the number of boutons with target-specific preferences. (**a**) Two models for the different average tuning of all boutons in AL and PM (see Fig. 2c). These differences may be due to the number of inputs, either axons or axonal branches, with matched properties (left; schematized by number of arrows) or area-specific biases in response amplitudes (right; schematized by the thickness of the arrows). (**b**) Cumulative distribution of preferred spatial frequency (SF; left), preferred temporal frequency (TF; middle) and peak speed (right) for all boutons imaged in each area in WT mice. (**c**) Same as in **b**, for boutons in Rbp4-cre mice. Dotted lines include boutons selected in AL with relaxed criteria ($P < 0.01$ for responsivity and 75% confidence intervals; $n = 143$). (**d**) Left, median speed of all boutons imaged in each WT (open circles) or Rbp4-cre (open triangles) mouse and for all boutons (filled circles). Areas imaged in the same mouse are connected with a gray line. Numbers of mice with each area imaged (black) and with multiple areas imaged (gray) are indicated below. Filled squares are the median speed of cell bodies imaged in AL (red) and PM (blue; from ref. 4). Right, cumulative distribution of peak speed for boutons (thick lines) and cell bodies (thin lines) imaged in AL and PM. Arrows at 10% and 90% highlight the difference in distributions at the low and high speeds.

Figure 6.
Areal bias in the amplitude of responses at different speeds is explained by the activity of a small fraction of boutons. (**a**) Two models for the different average tuning of all boutons in AL and PM (see Fig. 2c). These differences may be solely due to the number of inputs with matched properties (left; schematized by number of arrows) or extra, area-specific biases in response amplitudes (right; schematized by the thickness of the arrows). (**b**) Distributions of peak speeds for all boutons in AL and PM. (**c**) Average response amplitude (d*F*/*F*) for all boutons in AL and PM binned according to their peak speed. Boutons in AL with high peak speeds have a larger average response than boutons with low peak speeds; the opposite is true for boutons in PM. (**d**) Distributions of peak speeds for all boutons in each area, for different ranges of peak d*F*/*F*. Each bin notes the range of d*F*/*F* and the percentage of boutons from each area contained in that bin. The response preferences in AL and PM are segregated at all ranges of d*F*/*F*, but they become increasingly segregated for boutons with larger peak responses. (**e**) Average peak speed (top) and preferred spatial frequency (SF; middle) and temporal frequency (TF; bottom) for boutons grouped according to their peak d*F*/*F* (same bins as in **b**). All error bars, ± s.e.m.

Figure 7.
Axons projecting from LM to AL and PM are functionally distinct. (**a**) Tangential section of visual cortex after infection with GCaMP3 in LM. Scale bar, 500 μm; abbreviations as in Figure 1. (**b**) Example responses from six boutons from the same field of view in PM (top row) or AL (bottom row) of the same mouse. Boutons were ordered from lowest to highest speed and chosen as evenly spaced percentiles. Amplitude of d*F*/*F* is noted above each response. (**c**) Average response of all boutons (*n* represents number of boutons) in AL and PM for two example mice. (**d**) Average response for all boutons (top; *n* represents number of boutons) and for all mice (bottom; *n* represents number of mice) imaged in each area. (**e**) Average tuning curves for spatial frequency (SF; left), temporal frequency (TF; middle) and speed (right) for all boutons imaged in each area. Error bars, ± s.e.m. (**f**) Cumulative distribution of preferred SF (left), preferred TF (middle) and peak speed (right) for all boutons in AL and PM from LM (thick lines) and V1 (thin lines). (**g**) Median speed of all boutons from LM within each mouse (open circles) and for all boutons (filled circles). Areas imaged in the same mouse are connected with a gray line. Numbers of mice imaged in each area (black) and in both areas (gray) are given below. Filled squares are the median speed of boutons from V1 imaged in AL and PM (same data as in Fig. 5).